J Solid State Electrochem (2002) 6: 165–171
DOI 10.1007/s10008-001-0258-z

ORIGINAL PAPER

P. Knauth

Defect and transport properties of nanocrystalline ceramics and thin films

Received: 15 June 2001 / Accepted: 27 September 2001 / Published online: 29 November 2001
© Springer-Verlag 2001

Abstract This paper presents an overview of recent research on the defect and transport properties of nanocrystalline ionic and mixed conducting ceramics and thin films. In the first part, some basic concepts and properties of boundaries are reviewed, including diffusion, segregation, and space charge regions. Experimental data on nanoceramics and thin films made from pure and doped CeO_2, TiO_2, ZrO_2, and CaF_2 are presented and discussed in the second part; opportunities for future work on this topic are outlined.

Keywords Nanocrystalline ceramics · Thin films · Impedance spectroscopy · Ionic conductivity · Mixed conductivity

Introduction

Ceramics have been a part of human culture for thousands of years. From a scientific point of view, one can define ceramics as non-metallic polycrystalline materials, formed by compression and high-temperature sintering, typically above 1000 °C, of generally powdered precursors. In recent years, the trend to device miniaturization has favored the development of materials with at least one dimension in the nanometer scale. In this respect, thin films are one hot topic and nanocrystalline ceramics another. Nanocrystalline ceramics (''nanoceramics'') are dense compacts of small crystallites with a mean grain size below 100 nm [1]. Dense compacts of nanosized grains can be prepared by the hot-pressing technique, where forming and sintering are performed during a unique procedure, typically around 600 °C. Nanocrystalline ceramics present many advantages for applications, including the much lower sintering temperatures and improved mechanical properties, such as plastic deformation at relatively low temperature. Their properties have been intensely investigated for a number of years. The objective of this article is to review recent studies on defect and transport properties of ionic and mixed conducting nanoceramics [2, 3] and to check if general conclusions can already be drawn on these topics.

In the first part of this article we briefly recall defect and transport properties of interfaces, especially diffusion and segregation phenomena, which are paramount for the understanding and prediction of the experimental behavior of nanoceramics. In ionic materials, one has to distinguish between the interface core and the adjacent space charge regions, which result from the equilibrium redistribution of charged defects. In the second part, we present recent experiments on nanocrystalline electroceramics, including ZrO_2, CeO_2, TiO_2, and thin films based on CaF_2. We will try to evaluate which conclusions, if any, can be drawn on defect and transport properties of these materials and which experiments are needed in the future in order to shed more light on this domain.

Boundary properties

The exceptional properties of nanoceramics and thin films are obviously related to the high density of the interfaces. In the following, we review some of the key features of interfaces.

Boundary diffusion

Accelerated diffusion in the boundary core can be expected for two reasons: the large defect concentration at interface sites (high percentage of displaced atoms and strained bonds) and the large excess free volume, which enhances the defect mobility. In general, the activation

P. Knauth
MADIREL, Université de Provence-CNRS (UMR 6121),
Centre St. Charles, Case 26, 13331 Marseille Cedex 3, France
E-mail: knauth@up.univ-mrs.fr
Tel.: +33-491-106-296
Fax: +33-491-106-237

energy for interfacial diffusion is significantly lower than the bulk value, because defect formation and migration need less energy at interface sites. High-resolution electron micrographs of grain boundaries in oxides, e.g. NiO [4], show typically that the disordered region between grains is only a few atomic layers thick, not unlike the "grain boundary width" postulated for the interpretation of grain boundary diffusion data in metals (0.5 nm). Defects organize and create a new periodic interface structure with regularly repeating structural units. Ordinary boundaries are formed by portions of special boundaries.

In a polycrystalline material, the cross-sectional area of grain boundaries is normally very small. In an elementary brick model, the ratio of the cross-sectional areas of cubic grains of size L and grain boundaries (gb) of width d is:

$$A(\text{bulk})/A(\text{gb}) = L/2d \tag{1}$$

Grain boundary diffusion is the main diffusion contribution at low temperature and leads to a significant enhancement of mass transport in comparison with single crystals if the grain size is sufficiently small.

Grain boundary diffusion has been observed experimentally in many metallic systems [5]; in ionic compounds, however, experimental studies are few, because sample preparation and measurements are difficult, especially in refractory materials such as Al_2O_3. One can cite work on doped ZrO_2 [6], NiO and Al_2O_3 [7], and ZnO [8]. The classical experimental technique is radiotracer diffusion (e.g. ^{18}O in oxides).

Boundary segregation

Atoms or ions at interface sites have a different local environment than in the bulk (modified bond lengths, displaced atoms, etc.). In general, the chemical composition of an interface is therefore different from that of the bulk, the driving force being the minimization of the total free energy of the system (bulk + interfaces).

In ionic compounds, "intrinsic" segregation results from the different free enthalpies of defect formation at interface sites that can lead to an interfacial non-stoichiometry and a surface excess charge. Let us take the example of an oxide with predominant anion Frenkel disorder, written in the Kröger-Vink nomenclature [9]:

$$O_o + V_i \Leftrightarrow O_i + V_o^{\cdot\cdot} \tag{2}$$

If the free enthalpy of formation of vacancies is smaller than that of interstitials at a boundary, $G_f(V_o^{\cdot\cdot}) < G_f(O_i'')$, an excess of positive oxygen vacancies is observed; in other words, a positive boundary charge and oxygen deficiency (boundary reduction).

"Extrinsic" interfacial segregation of solutes (dopants and impurities) can have two driving forces. If a radius mismatch exists between host and solute ions, the elastic strain energy contributes to the driving force; a valence difference between host and solute ions leads to space charge layer segregation, as a consequence of the surface excess charge. In the previous example of a positive interface charge, the space charge layer is negatively charged, i.e. enriched in electrons and acceptor ions and depleted in electron holes and donor ions. Assumptions are that the solute is mobile at the temperature of the experiment and that the defect equilibrium is established, at least locally.

In the simplest case of a "Langmuir-McLean-type" segregation isotherm (assumptions: absence of electrostatic energy contributions, negligible solute interactions, and single type of interface site), the molar fraction of segregated solute at a grain boundary X_{gb} can be expressed by McLean's equation:

$$X_{gb} \Big/ \left(X_{gb}^{o} - X_{gb}\right) = [X_{bulk}/(1 - X_{bulk})]\ exp(-H_S/RT) \tag{3}$$

In this relation, X_{gb}^{o} corresponds to grain boundary saturation, X_{bulk} is the bulk molar fraction of solute, and H_S is the segregation enthalpy [10]. Even impurities present in the bulk at low concentration can reach a high interface concentration, provided that the segregation enthalpy is high enough.

Interfacial segregation has been investigated for metals [11] and different doped ceramic oxides, including MgO [12], TiO_2 [13], ZrO_2 [14], CeO_2 [15], and ZnO [16]. The most common surface analysis techniques applied in segregation studies are Auger electron spectroscopy (AES), X-ray photoelectron spectroscopy (XPS), and secondary ion mass spectrometry (SIMS).

Space charge regions

The formation of space charge layers is a consequence of local thermodynamic defect equilibria [17]. They have an important influence on the electrical properties of ceramics, because the space charge layer width can be orders of magnitude larger than the typical grain boundary core width of a few atomic distances. The space charge layer width is related to the Debye length:

$$\lambda^2 = \varepsilon\varepsilon_0 RT \Big/ \left[2F^2 \sum_i \left(z_i^2 [i]\right)\right] \tag{4}$$

In this equation, $\epsilon\ \epsilon_0$ is the permittivity, R and F the gas constant and Faraday's constant, T the absolute temperature, and $[i]$ the concentration of a charge carrier of charge z_i. From this relation, it is immediately clear that an enhancement of the charge carrier concentration, by appropriate doping or temperature increase, reduces the Debye length and thus the space charge layer width. Space charge effects are thus low-temperature effects and can gain considerable importance in systems with reduced charge carrier concentrations.

Maier [18] discussed the relevance of space charge effects for different ionic conducting materials: ionic conductor-insulator composites, thin films, and nanostructured materials. Particularly strong effects are expected when the Debye length becomes comparable to the grain size. In that case, the space charge regions begin to overlap; in other words, the "normal" bulk defect concentration is nowhere attained, not even in the grain center, and the grain is charged throughout (Fig. 1). This is equivalent to a change of the standard electrochemical potential. A "nanosize factor" g giving the supplementary conductivity enhancement was estimated for that case [19]:

$$g = 4\lambda/L \tag{5}$$

One of the goals of experimental studies is to check the validity of this prediction by studying systems with small grain size and low charge carrier concentration.

Segregation, diffusion, and space charge effects are interrelated and sometimes intricate; for example, charge carrier depletion in the grains by interface segregation of dopants can lead to an increase of the Debye length and, consequently, can enhance space charge effects. Interfacial diffusion is sensitive to solute segregation, and so on.

Nanoceramics and thin films

Microstructure and solute segregation

Structural investigations of nanocrystalline CeO_2 showed crystallites with a high degree of perfection, separated by sharp grain boundaries without indication of amorphous regions [20]. An EXAFS study of nanocrystalline ZrO_2 showed no major difference with microcrystalline materials, probably because strong ionic forces reduce any tendency to disorder [21]. The high order in the grain interior can be understood by the existence of a large number of interfaces, which can act as defect sinks, in atomic proximity. There is now sufficient evidence that grain boundaries in nanocrystalline materials are not significantly different from that of microcrystalline materials. The gas-like or glass-like grain boundary structure sometimes postulated in the early literature was not confirmed.

Given the high interface area, solute segregation in nanocrystalline materials can have important consequences. Copper segregation in nanocrystalline CeO_2 (grain size: ~18 nm) was investigated by e.m.f. measurements, using cells of the type $Cu,Cu_2O|CuBr|Cu_xCe_{1-x}O_{2-y}$ with CuBr as solid electrolyte at 320 °C [22]. X-ray diffraction suggested that Cu was dissolved in nanocrystalline CeO_2 up to $x = 0.15$. The thermodynamic activity of the copper oxides plotted against the copper molar fraction (Fig. 2) appears as a segregation isotherm with two plateaus. The second one above $x = 0.15$ corresponds to the apparent solubility limit of copper in nanosized ceria; it can be attributed to formation of a copper monolayer on the ceria nanoparticles. The materials with $x = 0.15$ show the highest catalytic activity for different redox gas reactions [23], confirming the importance of copper segregation for the exceptional catalytic properties of $Cu_xCe_{1-x}O_{2-y}$ nanoparticles.

The surface composition of nominally pure, Al- and Si-doped TiO_2 (anatase) nanoparticles was investigated by time-of-flight SIMS. There is clear evidence for Si segregation in pure and Si-doped TiO_2. In that case, the driving force for segregation is the elastic strain energy that can be estimated from the radius difference between Ti^{4+} and Si^{4+} ions (0.43 eV). The segregation of aliovalent Al^{3+} ions has elastic and electrostatic driving forces. In microcrystalline Al-doped TiO_2, previous investigations indicated space charge segregation of Al acceptor ions, because the TiO_2 surface presents an excess positive charge by oxygen vacancies, due to surface reduction [13]. SIMS and conductivity data on

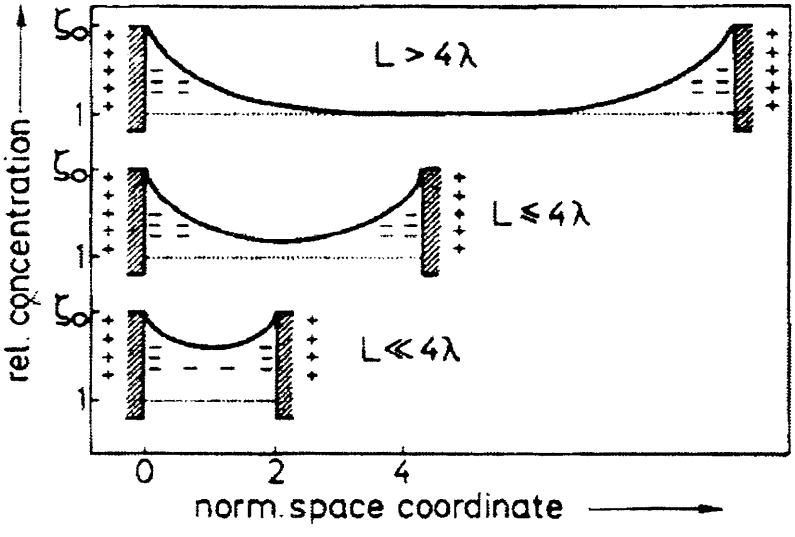

Fig. 1 Defect profiles within grains of size L. The bulk defect concentration is nowhere reached when $L < 4\lambda$, where λ is the Debye length (Eq. 4). An anomalous conductivity increase is then expected (mesoscopic effect). From [18]

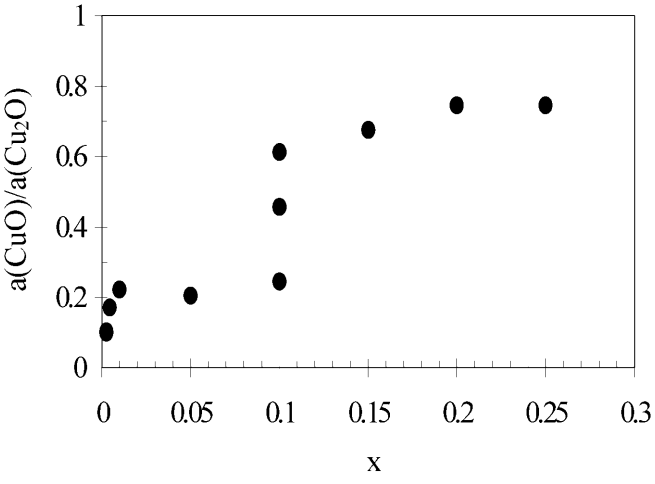

Fig. 2 Copper segregation isotherm in nanocrystalline $Cu_xCe_{1-x}O_{2-y}$. From [22]

nanocrystalline Al-doped samples can be interpreted by co-segregation of Al with Si impurities [24], which is not unexpected given that ordered 3D Al-Si-O compounds, such as mullite, exist.

Electrical properties are also very sensitive to interfacial segregation: Ca and Si segregation in stabilized ZrO_2 has been correlated with variations of the blocking grain boundary conductivity, i.e. the conductivity across the grain boundary [14]. One has always to take into account the anisotropy of interface properties and separate transport along and across interfaces. For microcrystalline materials, this is possible by impedance spectroscopy, because the different capacitances of bulk and grain boundary regions lead to a significant difference of the time constants of transport along and across a grain boundary that ensures a clear separation in the complex impedance plane. A significant enhancement of the blocking grain boundary conductivity was observed at grain sizes below 2 μm, because the grain boundary coverage by segregated solutes obviously decreases with decreasing grain size. In nanocrystalline materials, solute segregation occurs on a much larger grain boundary area and the mean grain boundary concentration of segregated solutes is much lower than in microcrystalline materials with the same solute content. This should further enhance the specific grain boundary conductivity in nanoceramics. Indeed, nanocrystalline tetragonal ZrO_2 doped with 1.7 and 2.9 mol% Y_2O_3 (average grain size: 40–50 nm) have a blocking grain boundary conductivity 1–2 orders of magnitude higher than comparable microcrystalline samples, with a low activation energy (1.03 ± 0.03 eV), which is grain-size independent. Both results can be attributed to the reduced grain boundary concentration of Si [25]. The specific grain boundary conductivity of fully dense CeO_2 nanoceramics (mean grain size: 10 nm) [20] is orders of magnitude higher than in microcrystalline samples. Tschöpe et al. [26] observed similar results in samples with a mean grain size of 26 nm. In rutile TiO_2 nanoceramics (grain size: 40–50 nm), the specific grain boundary conductivity is about 200 times larger than that of conventional microcrystalline samples [27].

Altogether, the enhancement of the blocking grain boundary conductivity seems to be a general observation; the dilution of segregated impurities over the much larger grain boundary area in nanocrystalline materials appears to be a consistent explanation.

Electronic conductivity and non-stoichiometry

Nanocrystalline CeO_2 [20] remains an n-type semiconductor even at high oxygen partial pressure, in contrast to conventional microcrystalline samples that are ionically conducting, due to acceptor doping. The electronic conductivity is about four orders of magnitude larger than for conventional samples at high $P(O_2)$. The activation energy is reduced by more than a factor of 2 (1.1 vs. 2.5 eV [20]). In the work by Tschöpe et al. [26] on CeO_2 nanoceramics, the electronic conductivity was enhanced by about 20 and the activation energy was also reduced, but less (1.7 eV). Kosacki and co-workers [28] found a significant conductivity enhancement for CeO_2 thin films and investigated the lattice disorder by Raman spectroscopy. Tschöpe [29] recently proposed a model that explains the increase of electronic conductivity and decrease of ionic conductivity, based on the space charge layer concept. Assuming a positive boundary charge due to reduction (see above), the space charge regions should be enriched in electronic carriers (excess electrons), but depleted in ionic carriers (oxygen vacancies). The model calculations predict that the activation energies for ionic and electronic conduction are grain-size dependent: with decreasing grain size, it should increase for the ionic conductivity and decrease for the electronic part. This model consistently explains the enhanced activation energy for ionic conduction in CeO_2 nanoceramics (1.6 eV, about twice the value for microcrystalline CeO_2), found by Mason and co-workers [30].

On the other hand, the enhancement of electronic conductivity observed by Chiang et al. [20] can be explained by assuming that the enthalpy of the reduction reaction is significantly lower at interface sites (2 eV vs. 4.7 eV in conventional CeO_2):

$$O_o \rightarrow V_o^{\cdot\cdot} + 2e' + \frac{1}{2}O_2(g) \qquad (6)$$

The striking enthalpy decrease implies a corresponding enhancement of the oxygen deficiency to values of the order of 10^{-6}–10^{-5}, in comparison with 10^{-9} for conventional samples. The fraction of reduced interface oxygen sites can be estimated from the surface-to-volume ratio for 10 nm grain size: only one out of 10,000 grain boundary sites needs to be reduced to dominate the defect and transport behavior of the nanoceramics. Using coulometric titration with oxygen solid electrolyte cells, Porat et al. [31] indeed found a large oxygen deficiency in nanocrystalline CeO_2, up to values of 10^{-3}.

Nanocrystalline Pr-doped CeO_2 samples have an even higher, exceptional, oxygen deficiency ($x > 0.1$ at 640 °C; Fig. 3 [37]), because of the easy valence change of Pr^{4+}/Pr^{3+} ions and the existence of many interfaces. Furthermore, the high interface density improves the oxygen exchange kinetics, especially the oxygen diffusivity (see below).

Dense nanocrystalline anatase TiO_2 ceramics with a mean grain size of 35 nm show a high electronic conductivity with strong partial pressure exponent (–1/2) at low oxygen partial pressure and a conductivity plateau at high $P(O_2)$ (Fig. 4 [32]). The large pressure dependence at low $P(O_2)$ is certainly of interest for sensor applications. The exponent can be interpreted by assuming that the majority ionic defects are not completely ionized; in other words, that the concentrated ionic ($Ti_i^{\cdot\cdot}$) and electronic defects (e') are associated. The reduction reaction can be written:

$$TiO_2 \rightarrow Ti_i^{\cdot\cdot} + 2e' + O_2(g) \quad (7)$$

The reduction enthalpy (7.8 eV) is lower than in conventional microcrystalline TiO_2 (~10 eV), indicating a reduced defect formation enthalpy at interface sites. Given the large background acceptor concentration (Na^+), the Debye length is certainly small so that important space charge effects are not expected in these samples.

For the moment, it is difficult to decide which model, reduced defect formation energies at interface sites or existence of space charge regions, is more appropriate to describe the behavior of nanoceramics; probably this depends on individual experimental parameters, including impurity concentrations, etc. Definitely more work is necessary; the grain size dependence of the activation energies should be especially studied.

Diffusion and ionic conductivity

Quite surprisingly, there are not many investigations showing enhanced diffusion or ionic conduction in nanoceramics and thin films.

^{18}O diffusion profiles in nominally undoped fully dense nanocrystalline ZrO_2 with monoclinic structure show grain boundary diffusion at deeper penetration [33]. Within the entire temperature range between 450 and 950 °C, the grain boundary diffusion coefficients, $D_{gb} = 0.3\exp(-1.95\,eV/kT)$, are 3–4 orders of magnitude higher than the bulk diffusion coefficients, $D_{bulk} = 0.002\exp(-2.3\,eV/kT)$. The latter are similar to earlier results on coarse-grained monoclinic samples. However, the grain boundary diffusion coefficient in nanocrystalline monoclinic ZrO_2 remains below the diffusion coefficient in conventional Ca- (CSZ) or Y-stabilized zirconia (YSZ), which are due to the high doping-related vacancy concentration. A worthwhile study of the oxygen diffusivity in cubic YSZ nanoceramics is in progress (Routbort J, personal communication).

In dense tetragonal ZrO_2 nanoceramics doped with Y, similar levels of ionic conductivity to those found in conventional samples were obtained, whereas thin films of cubic Y (16 mol%)-doped ZrO_2 showed enhanced ionic conductivity by one order of magnitude with a low

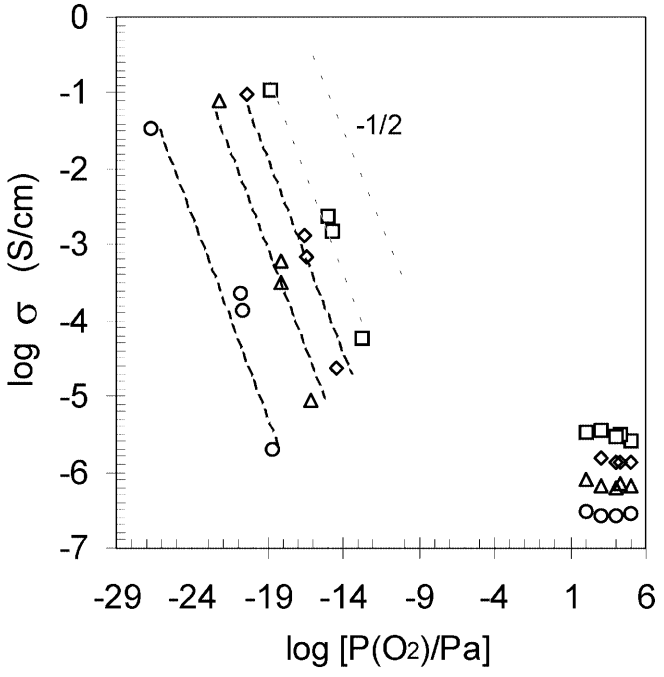

Fig. 3 Relative oxygen deficiency (x–x_0) of $Pr_{0.7}Ce_{0.3}O_{2-x}$ at 470 (*open circles*), 560 (*squares*), and 640 °C (*filled circles*) as a function of the oxygen partial pressure. From [37]

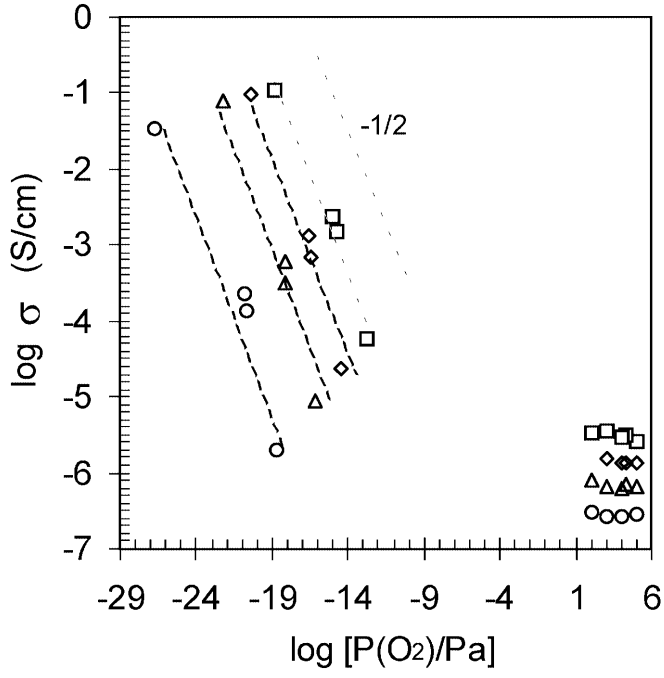

Fig. 4 Oxygen partial pressure dependence of the electrical conductivity of anatase nanoceramics at 450 (*circles*), 500 (*triangles*), 530 (*squares*), and 580 °C (*diamonds*). From [32]

activation energy (0.93 eV) [34]. This discrepancy suggests the possibility of substrate effects on thin films. Recently, nanocrystalline tetragonal ZrO_2 films were successfully prepared using electrostatic spray deposition [35] and the grain size effect on the tetragonal-monoclinic phase transition was studied by Raman spectroscopy and X-ray diffraction [36]. More investigations of the electrical properties of ZrO_2 thin films are worthwhile.

On highly doped nanocrystalline $Pr_{0.7}Ce_{0.3}O_{2-x}$, coulometric titration experiments using oxygen concentration cells gave high chemical diffusion coefficients with an exceptionally low activation energy (0.3 eV; Fig. 5 [37]). This might reflect the existence of a large density of fast interface diffusion paths with reduced defect migration energy. However, this conclusion remains to be validated for other solid solutions and by different techniques.

The existence of a conductivity plateau at high oxygen partial pressure indicates a domain of predominant ionic conduction with a plausible activation energy (~1 eV; Fig. 6) in nanocrystalline TiO_2 (anatase). Nowotny et al. [38] found predominant ionic conduction in a rutile single crystal around 900 °C, with a significantly higher activation energy (1.6 eV). These results can be attributed to the existence of a large density of interfacial diffusion paths with reduced migration energy in the nanoceramics, where ionic transport is enhanced. Demetry and Shi [27] prepared rutile nanoceramics (grain size: 40–50 nm) with the addition of about 1 mol% SnO_2. Some similarities with the anatase data exist; for example, a conductivity plateau at high $P(O_2)$, indicating ionic conduction with an identical activation energy (~1 eV). Clearly, the confirmation of the ionic conductivity in TiO_2 by e.m.f. measurements is worthwhile.

CaF_2 nanoceramics (grain size: 9 nm) have an increased ionic conductivity that can be understood by scaling up the space charge effects observed in conventional materials [39]. A systematic deviation at the highest temperature can be related to grain coarsening during the experiments. The activation energy corresponds to the migration energy of fluoride vacancies and suggests an accumulation of F^- vacancies in the space charge regions. Given the Na background concentration, the computed Debye length (1 nm) is well below the grain size, so that an observation of mesoscopic space charge effects is not expected; it requires highly pure nanocrystalline samples.

This objective was recently attained by the preparation of epitaxial CaF_2/BaF_2 heterolayers by molecular beam epitaxy (MBE) on alumina substrates at 500 °C [40]. The multilayer period was varied between 16 and 430 nm with an overall thickness of 500 nm. The parallel conductivities increase linearly with the number of heterojunctions, provided that the period is greater than 100 nm. The films with smaller periods exhibit an anomalous conductivity increase. Calculation of the Debye length (15 nm) revealed that this effect is related to an overlap of space charge regions.

At low temperature, the activation energy is dominated by BaF_2, in accordance with the larger vacancy mobility in this compound, whereas the activation energy at higher temperature seems to be determined by space charge layer conduction in CaF_2. This indicates a transfer of F^- ions from BaF_2 to CaF_2 rather than phase boundary core segregation of F^- ions. This study is the first case where mesoscopic space charge effects are experimentally demonstrated, although the existence of mesoscopic ionic heterolayers was already postulated to describe the very high ionic conductivity of $AgI\text{-}Al_2O_3$ composites [41].

Conclusions

What are the conclusions concerning defect and transport properties of nanocrystalline ceramics after the first 10 years of studies?

There is no indication for a gas-like or glass-like grain boundary structure in nanocrystalline ceramics. The grain interior shows high perfection.

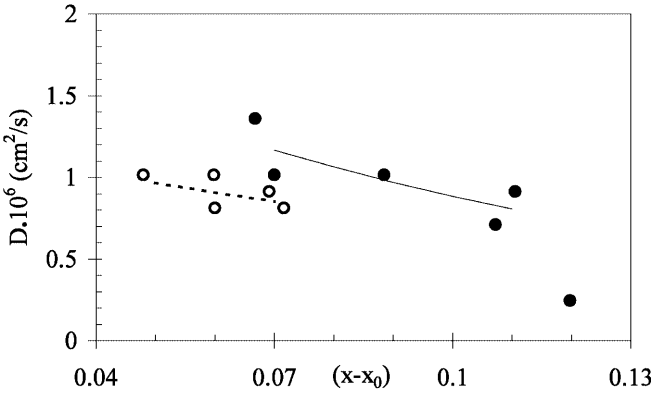

Fig. 5 Chemical diffusion coefficients of $Pr_{0.7}Ce_{0.3}O_{2-x}$ at 560 (*open circles*) and 640 °C (*filled circles*) as a function of the relative oxygen deficiency (x–x_0). From [37]

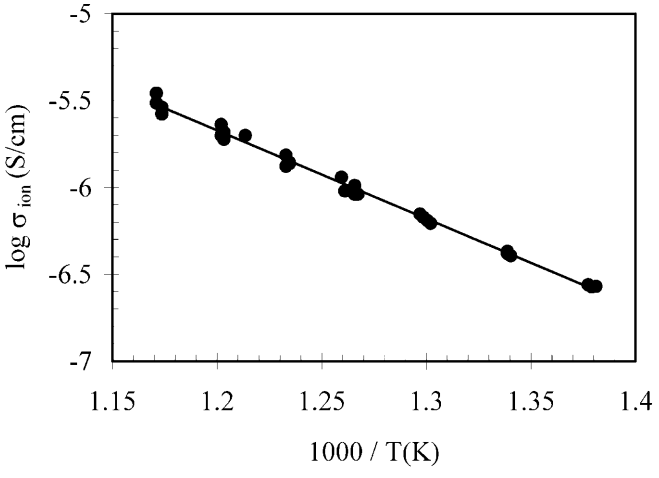

Fig. 6 Arrhenius plot of the ionic conductivity of TiO_2 (anatase) nanoceramics. From [32]

There is convincing evidence that the blocking grain boundary conductivity is significantly enhanced, because of size-dependent solute segregation. This can be fundamental for applications, where a high conductivity is of importance. Solute segregation was also shown to be decisive for the catalytic properties of nanoparticles.

A significant enhancement of the electronic conductivity of nanocrystalline oxides can be related to the high density of interface sites, where defect formation energies are reduced. However, the significance of space charge effects must be investigated closer. Anyway, these results are interesting for conductometric oxygen sensors.

Only a few investigations showed enhanced diffusion and ionic conduction in nanoceramics and thin films. In oxides, these experiments need to be confirmed by independent methods, especially e.m.f. measurements using oxygen concentration cells.

The existence of overlapping space charge layers and the associated anomalous increase of ionic conductivity (nanosize factor) was experimentally verified for ionic heterostructures with small periodicity.

However, the most obvious conclusion is that our knowledge on nanocrystalline materials is insufficient. Many more investigations are necessary: ''There's plenty of room at the bottom.'' (R. Feynman, 1959).

Acknowledgements The author acknowledges the financial support for this research in the framework of the CNRS-NSF cooperative research agreement.

References

1. Gleiter H (2000) Acta Mater 48:1
2. Knauth P, Tuller HL (1999) Mater Res Soc Symp Proc 548:429
3. Schoonman J (2000) Solid State Ionics 135:5
4. Merkle KL (1994) J Phys Chem Solids 55:991
5. Sutton AP, Balluffi RW (1995) Interfaces in crystalline materials. Oxford University Press, New York
6. Kingery WD, Pappis J, Doty ME, Hill DC (1959) J Am Ceram Soc 42:393
7. Atkinson A (1988) Solid State Ionics 28–30:1377
8. Tuller HL (1999) J Electroceram 4:S1:33
9. Kröger F (1974) The chemistry of imperfect crystals, 2nd edn. North-Holland, Amsterdam
10. McLean D (1957) Grain boundaries in metals. Clarendon, Oxford, p 116
11. Seah MP, Hondros ED (1973) Proc R Soc London Ser A 335:191
12. Chiang YM, Henriksen AF, Kingery WD, Finello D (1981) J Am Ceram Soc 64:385
13. Ikeda JAS, Chiang YM, Garratt-Reed AJ, Vander Sande JB (1993) J Am Ceram Soc 76:2447
14. Aoki M, Chiang YM, Kosacki I, Lee LJR, Tuller HL, Liu Y (1996) J Am Ceram Soc 79:1169
15. Blom DA, Chiang YM (1997) Mat Res Soc Symp Proc 458:127
16. Lee JR, Chiang YM, Ceder G (1997) Acta Mater 45:1247
17. Lehovec K (1953) J Chem Phys 21:1123
18. Maier J (1995) Prog Solid State Chem 23:171
19. Maier J, Prill S, Reichert B (1988) Solid State Ionics 28–30:1465
20. Chiang YM, Lavik EB, Kosacki I, Tuller HL, Ying JY (1997) J Electroceram 1:7
21. Rush GE, Chadwick AV, Kosacki I, Anderson HU (2000) J Phys Chem B 104:9597
22. Knauth P, Schwitzgebel G, Tschöpe A, Villain S (1998) J Solid State Chem 140:295
23. Tschöpe A, Ying JY, Tuller HL (1996) Sens Actuators B 31:111
24. Knauth P, Auer G (2001) Solid State Ionics (submitted)
25. Mondal P, Klein A, Jaegermann W, Hahn H (1999) Solid State Ionics 118:331
26. Tschöpe A, Sommer E, Birringer R (2001) Solid State Ionics 139:255
27. Demetry C, Shi X (1999) Solid State Ionics 118:271
28. Suzuki T, Kosacki I, Anderson HU, Colomban P (2001) J Am Ceram Soc 84:2007
29. Tschöpe A (2001) Solid State Ionics 139:267
30. Mason TO, Hwang JH (1998) Z Phys Chem 207:21
31. Porat O, Tuller HL, Lavik EB, Chiang YM (1997) In: Komarneni S, Parker J, Wollenberger H (eds) Nanophase and nanocomposite materials II. Materials Research Society, Pittsburgh, p 99
32. Knauth P, Tuller HL (1999) J Appl Phys 85:897
33. Schaefer HE, Reimann K, Straub W, Phillipp F, Tanimoto H, Brossmann U, Würschum R (2000) Mater Sci Eng A 286:24
34. Kosacki I, Suzuki T, Petrovsky V, Anderson HU (2000) Solid State Ionics 136–137:1225
35. Nguyen T, Djurado E (2001) Solid State Ionics 138:191
36. Djurado E, Bouvier P, Lucazeau G (2000) J Solid State Chem 149:399
37. Knauth P, Tuller HL (1999) J Eur Ceram Soc 19:831
38. Nowotny J, Radecka M, Rekas M, Sugihara S, Vance ER, Weppner W (1998) Ceram Int 24:571
39. Puin W, Rodewald S, Ramlau R, Heitjans P, Maier J (2000) Solid State Ionics 131:159
40. Sata N, Eberman K, Eberl K, Maier J (2000) Nature 408:946
41. Lee JS, Adams St, Maier J (2000) Solid State Ionics 136–137:1261